

# Molecular Perspective on Water Vapor Accommodation into Ice and Its Dependence on Temperature

Daniel Schlesinger,\* Samuel J. Lowe, Tinja Olenius, Xiangrui Kong, Jan B. C. Pettersson, and Ilona Riipinen\*

Cite This: *J. Phys. Chem. A* 2020, 124, 10879–10889

Read Online

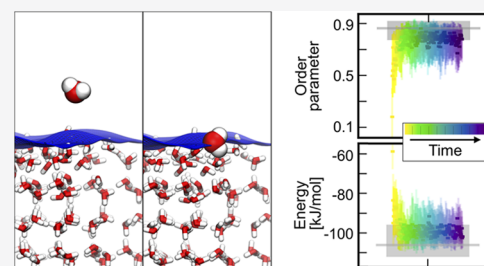
ACCESS |

Metrics & More

Article Recommendations

Supporting Information

**ABSTRACT:** Accommodation of vapor-phase water molecules into ice crystal surfaces is a fundamental process controlling atmospheric ice crystal growth. Experimental studies investigating the accommodation process with various techniques report widely spread values of the water accommodation coefficient on ice,  $\alpha_{ice}$ , and the results on its potential temperature dependence are inconclusive. We run molecular dynamics simulations of molecules condensing onto the basal plane of ice  $I_h$  using the TIP4P/Ice empirical force field and characterize the accommodated state from this molecular perspective, utilizing the interaction energy, the tetrahedrality order parameter, and the distance below the instantaneous interface as criteria. Changes of the order parameter turn out to be a suitable measure to distinguish between the surface and bulk states of a molecule condensing onto the disordered interface. In light of the findings from the molecular dynamics, we discuss and re-analyze a recent experimental data set on  $\alpha_{ice}$  obtained with an environmental molecular beam (EMB) setup [Kong, X.; et al. *J. Phys. Chem. A* 2014, 118 (22), 3973–3979] using kinetic molecular flux modeling, aiming at a more comprehensive picture of the accommodation process from a molecular perspective. These results indicate that the experimental observations indeed cannot be explained by evaporation alone. At the same time, our results raise the issue of rapidly growing relaxation times upon decreasing temperature, challenging future experimental efforts to cover relevant time scales. Finally, we discuss the relevance of the water accommodation coefficient on ice in the context of atmospheric cloud particle growth processes.



## 1. INTRODUCTION

Condensation and deposition of water vapor onto liquid water and ice surfaces is a key process in the Earth's atmosphere, driving, e.g., the growth of cloud droplets and ice crystals and hence influencing the evolution and properties of clouds.<sup>1,2</sup> The key parameter governing the thermodynamic equilibria between water vapor and its various condensed phases is the saturation vapor pressure above the liquid or solid phase, which is directly linked to the evaporation rate of water molecules from the condensed phase.<sup>1–3</sup> The difference between the ambient water vapor concentration and the equilibrium vapor pressure determines to a large degree the net growth or evaporation of water hydrometeors.<sup>1,2</sup> An additional coefficient known as the mass accommodation coefficient  $\alpha$  (also sometimes called the condensation or evaporation coefficient) has been proposed to modulate the condensation and evaporation fluxes at the free molecular regime.<sup>3,4</sup> The most common formulation defines  $\alpha$  as the fraction of incoming molecules, as determined by kinetic gas theory, that stick and accommodate into the bulk condensed phase in the absence of evaporation, or in reverse, the ratio between the evaporation rate and the maximum kinetic evaporation into vacuum (i.e., in the absence of condensation or deposition).<sup>3,5</sup> Being a primarily kinetic parameter, the effect of  $\alpha$  disappears

at the limit of the continuum regime where the condensation or deposition becomes diffusion-limited and can thus be described by the macroscopic transport equations (see, e.g., ref 6 and references therein). In the literature investigating water condensation, deposition, and evaporation, however, the definition and physical interpretation of the mass accommodation coefficient vary. Most studies relate  $\alpha$  to an additional energetic barrier related to the restructuring of the surface as it takes up a molecule.<sup>6,7</sup> For ice surfaces, the mass accommodation coefficient is alternatively related to a reorientation of the condensing molecule.<sup>8</sup> Some studies describe particle-phase transport through an effective mass accommodation coefficient (e.g., refs 9, 10). The uptake coefficient, often denoted with  $\gamma$ , can be used from the free molecular to the continuum regimes, and it converges with  $\alpha$  in the kinetic regime.<sup>11</sup> The ambiguity in the definition of  $\alpha$  makes it difficult to compare and interpret experimental data,

Received: October 15, 2020  
Revised: December 5, 2020  
Published: December 15, 2020



and eventually resolve the value of  $\alpha$  that should be used in, e.g., cloud models.<sup>12</sup> Furthermore, it is not fully clear in which conditions the accommodation process can be described by a single accommodation parameter  $\alpha$ , instead of treating it as a two-step process governed by the separate surface and bulk accommodation coefficients  $\alpha_s$  and  $\alpha_b$ .<sup>13,14</sup> Such a description is particularly relevant for nonhomogeneous, multilayered surfaces such as ice, in which a disordered interface<sup>15</sup> separates the crystalline ice from the vapor phase.<sup>16</sup>

For liquid water, numerous experimental and theoretical studies of  $\alpha$  find values close to unity (e.g., refs 17–19), while others find significantly lower values (see, e.g., ref 5). Accurately constraining  $\alpha$  has proven challenging with standard experimental techniques due to, e.g., uncertainty in other key parameters needed for the interpretation of the data, especially evaporation rates, diffusion coefficients, and the ambient water vapor concentration and temperature.<sup>17</sup> Julin et al.<sup>14</sup> studied the condensation and evaporation of water with a combination of molecular dynamics (MD), kinetic modeling, and experimental data at  $T = 268$ – $300$  K and concluded that their results were in line with  $\alpha > 0.99$  for both planar and curved surfaces. Furthermore, it was concluded that simple kinetic modeling representing the accommodation process without explicitly accounting for the surface phase (i.e., as a one-step process with a single  $\alpha$ ) was sufficient. In the case of ice, however, accommodation involves the disordered interface. Close to the melting temperature  $T_m$ , this interface is often referred to as the “premelting layer” or the “quasi-liquid layer”, and its thickness and properties strongly depend on temperature.<sup>20,21</sup> Upon cooling below  $T_m$ , the thickness quickly drops to molecular dimensions and at temperatures far below  $T_m$ , i.e.,  $T_m - T \gtrsim 25$  K, only the topmost molecular layer is affected by entropic disordering.<sup>22,23</sup> Here, we investigate the role of this disordered layer in the accommodation process, treating the accommodation process to the surface vs uptake to the bulk crystal as separate processes manifested in different  $\alpha_s$  and  $\alpha_b$ , respectively.

A wide range of experimental techniques have been applied in the past decades for probing the condensation and evaporation of water vapor on and from ice and extracting an accommodation coefficient. These techniques include various molecular beam-based approaches,<sup>24–27</sup> Fourier transform infrared (FTIR) spectroscopy,<sup>28</sup> optical interference,<sup>26,29</sup> use of electrodynamic balance in controlled vapor concentrations,<sup>30</sup> microbalances and/or mass spectrometric techniques coupled to different flow reactors, vacuum chamber or Knudsen cell designs<sup>31–37</sup> as well as monitoring the evolution of aerosol particles and hydrometeors in flow tubes or condensation/evaporation chambers.<sup>38–40</sup> In general, the techniques applied for assessing the accommodation coefficient at higher temperatures tend to report on average lower values than the approaches focusing on lower temperatures (see, e.g., Kong et al.<sup>27</sup>). A decreasing temperature trend using the same technique throughout the temperature range has been reported by, e.g., Delval et al.,<sup>35</sup> Pratte et al.,<sup>37</sup> and Kong et al.<sup>27</sup> for 120–240 K. On the other hand, Magee et al.<sup>30</sup> and Choularton and Latham<sup>39</sup> reported an increasing trend with temperature range 190–260 K. Some studies, like Kramers and Stemerding<sup>31</sup> for 213–233 K, Haynes et al.<sup>29</sup> for 20–185 K, and Skrotzki et al.<sup>40</sup> for 190 and 235 K, reported values close to unity with practically no temperature dependence at all. The differences between the values obtained by different measurement approaches can result from uncertainties in the

measurable quantities or, e.g., potential measurement artifacts. However, the ambiguities in the mere definition of the accommodation coefficient might play a role in the variation of the observation results. As the definition is built on the models that are used to link the directly measurable quantities to the underlying physical processes, variations in the approach for interpreting the measurements may contribute to the deviations in the values deduced for  $\alpha$ .

Molecular dynamics (MD) simulations are a useful tool for addressing surface processes and particularly valuable for identifying the molecular and structural properties manifesting themselves as an accommodation coefficient (see, e.g., ref 14). While such simulations are challenging to perform for ice at low temperatures, since the relaxation times are long compared to feasible simulation times, they are applicable for the ice interface, where the characteristic time scales lie between those of the corresponding supercooled liquid and the solid. MD simulations have been applied by Neshyba et al.<sup>16</sup> to study the adsorption and bulk accommodation processes of water molecules on an ice (0001) surface involving the disordered layer, reporting values for the surface accommodation coefficient of  $\alpha_s > 0.99$  and the bulk accommodation coefficient of  $\alpha_b = 0.6$  at  $T = 250$  K using a six-site water model. These authors define the surface accommodation coefficient as the fraction of condensing molecules sticking to the surface, while the bulk accommodation coefficient was calculated from the ratio of transitions between the quasi-liquid layer into the bulk layer and transitions between the quasi-liquid layer into bulk and vapor phase. The authors emphasize, however, that this result depends on the choice of the layer in which the accommodation is assumed to take place. In a more recent study, MD simulations were used to inspire a continuum description of ice crystal growth dynamics, which takes the quasi-liquid and faceted structure of the ice surface into account.<sup>41</sup> Mohandesi and Kusalik focused on the ice growth rate from the vapor phase as obtained from MD simulations of the TIP4P/2005 model of water,<sup>42</sup> obtaining the temperature-dependent ice growth rate with maxima of 7 cm/s for the prism face and 4 cm/s for the basal face, respectively. The latter study did not attempt to obtain a bulk accommodation coefficient although information about it must be contained in the data. Llombart et al. have furthermore investigated the role of nitrogen gas above the ice surface and found that collisions with the carrier gas can lead to an effective slowdown of the water vapor flux toward the ice interface.<sup>43</sup>

In this paper, we use a combination of MD simulations and kinetic flux calculations to develop a molecular definition of  $\alpha$  for water vapor over ice over a wide temperature range, exploring the influence of the disordered interface on the accommodation process. In contrast to most previous studies, we use the instantaneous interface as a reference and obtain distributions of the tetrahedrality order parameters and the interaction energies as a function of distance below this interface. First, we study the properties of bulk ice as compared with the surface and vapor phases to establish criteria for when a molecule can be considered to be accommodated as part of the surface or the bulk ice. Second, we follow an ensemble of trajectories of molecules originating from the gas phase as they penetrate into the condensed phase, comparing the time evolution of their energetics and orientation to the criteria established for surface and bulk accommodation. Finally, we explore potential uncertainties in interpreting experimental data on accommodation through a case study of analyzing the

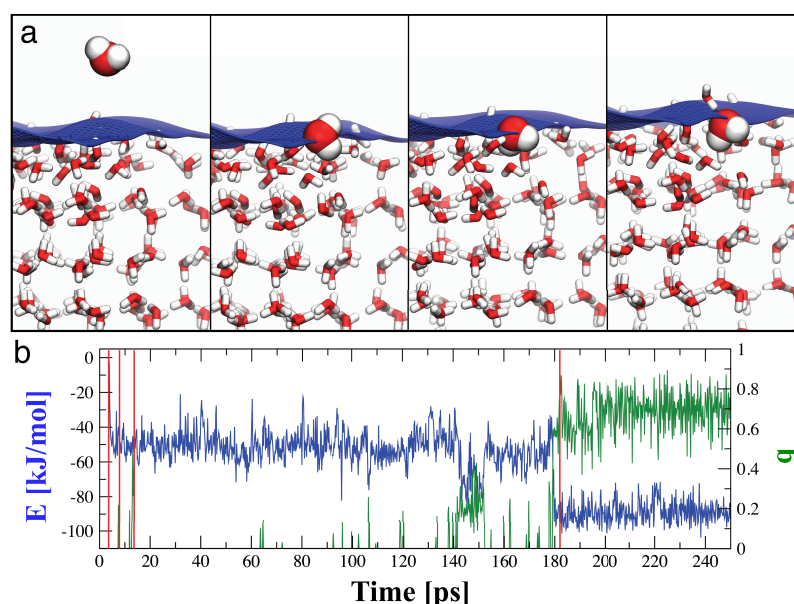


**Figure 1.** (a) Snapshots from a simulation of a condensing molecule on an ice surface at  $T = 200$  K at simulation times  $t = 3.4, 7.6, 13.4,$  and  $182$  ps (left to right). We use a different representation for the condensing molecule than for bulk molecules for clarity. The instantaneous interface indicated in blue is computed using the procedure described in Section 2. The snapshots were rendered with VMD.<sup>49</sup> (b) Short-range interaction energy  $E$  (left vertical axis, blue line) and tetrahedrality parameter  $q$  (right vertical axis, green line) from the first 250 ps of a simulation at  $T = 200$  K as functions of time. The times at which the snapshots of panel (a) are taken are indicated with red vertical lines at  $t = 3.4, 7.6, 13.4,$  and  $182$  ps.

data from Kong et al. with a kinetic flux modeling approach using insights from the molecular simulations.

## 2. METHODS

**2.1. Molecular Dynamics Simulations.** Here, we focus on the accommodation process of single molecules condensing onto ice surfaces at different temperatures. We use the program package GROMACS ver. 5.1.4<sup>44</sup> and the TIP4P/Ice model of water<sup>45</sup> to simulate systems initially containing a slab of ice ( $N = 432$  molecules) and one gas-phase molecule (Figure 1a) at temperatures of  $T = 100, 170, 200, 230,$  and  $250$  K, the melting temperature of TIP4P/Ice being  $T_m = 272.2$  K.<sup>45</sup> The ice slabs are equilibrated prior to the production runs for  $t_{\text{eq}} = 100$  ns ( $T = 100, 170,$  and  $200$  K) and  $t_{\text{eq}} = 10$  ns ( $T = 230$  and  $250$  K). After the initial equilibration in the isothermal–isobaric (NPT) ensemble using the Parrinello–Rahman barostat,<sup>46</sup> 100 frames are extracted from the trajectories at each temperature.

For each of the 100 configurations, we add a gas-phase molecule approximately  $\Delta z \approx 2$  nm above the surface with velocities initialized according to the Maxwell–Boltzmann distribution at the respective temperature  $T$  and switch to the canonical (NVT) ensemble. All molecules, excluding the vapor-phase molecule, are coupled to a heat bath using the Bussi thermostat<sup>47</sup> and propagated in time at a time step of  $dt = 2$  fs for total simulation times of 10 ns ( $T = 200, 170, 100$  K), 2 ns ( $T = 230$  K), and 1 ns ( $T = 250$  K). After velocity initialization, the condensing molecule is not coupled to the thermostat at any time. Coulomb interactions are treated with the particle-mesh Ewald method (see, e.g., ref 48).<sup>48</sup> Both van der Waals and real-space Coulomb interactions are cut off at 0.85 nm. We use three different indicators for characterizing the accommodation process: the distance to the instantaneous interface, the short-range interaction energy, and an order parameter.

**2.1.1. Definition of the Surface.** The instantaneous surface of the ice slab is defined as the half bulk-density iso-surface of the density field obtained by adding contributions from Gaussians, centered around each oxygen atom, on a  $50 \times 50 \times 50$  points 3-D grid following the method detailed in ref 50. This definition allows us to measure the distance of the condensing molecule to the surface, which is rough on a molecular level, and to plot other characterizing quantities, such as the order parameter, as a function of the distance. The condensing molecule is omitted from the determination of the surface and can thus appear to locally deform the interface. The result of this analysis is illustrated in Figure 1a. Although this method was originally introduced for liquid interfaces, it is used here for ice surfaces as it is a robust method regardless of the degree of disorder in the interface.

**2.1.2. Definition of the Order Parameter.** The order parameter characterizing the orientation of molecule  $i$  with respect to the surrounding molecules is here defined as the tetrahedrality parameter

$$q_i = 1 - \frac{3}{8} \sum_j^3 \sum_{k=j+1}^4 \left( \cos \psi_{jk} + \frac{1}{3} \right)^2 \quad (2.1)$$

similar to the definition in ref 51 (see also Figure 1b for an example), but without thermal averaging.  $\psi_{jk}$  denote the angles between the lines connecting the oxygen atoms of the central molecule  $i$  with those of its nearest neighbors  $j$  and  $k$ . The original order parameter from ref 51 is unity for perfectly tetrahedral configurations, i.e., an ideal ice lattice, and vanishes for random configurations. In our case, without thermal averaging,  $q_i \in [-3, 1]$ , but the value  $q_i \approx 1$  for tetrahedral configurations still holds. Therefore, for molecules occupying undisturbed ice lattice sites,  $q_i = 1$ , while we define  $q_i := 0$  for molecules with less than four neighbors within a cutoff distance of  $d_{\text{cut}} = 3.7$  Å. We only consider values of  $0 \leq q_i \leq 1$  and omit possible negative values since the corresponding highly

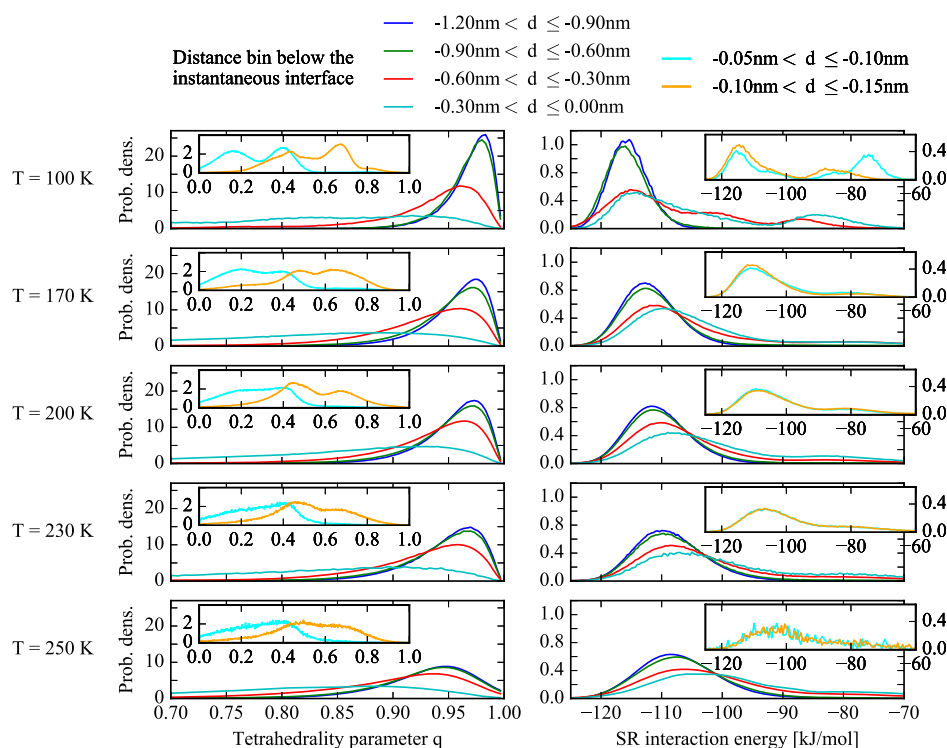


**Figure 2.** Tetrahedrality parameter and interaction energy distributions for 3 Å thick layers (distance bins) below the instantaneous interface for all temperatures simulated. The insets show tetrahedrality parameter and interaction energy distributions for two thinner layers of 0.5 Å thickness right below the instantaneous interface.

distorted local H-bond structures are not of interest in the current context. We will refer to the order parameter as “tetrahedrality parameter”  $q$ .

**2.1.3. Definition of the Short-Range Interaction Energy.** The transition of a molecule from the vapor to the condensed phase can be characterized by the intermolecular interaction energy. During the transition, the interaction energy changes from no, or weak, interactions to strong attractive interactions. Here, we use the short-range (SR) interaction energy, i.e., the sum of Coulomb and van der Waals interactions, of a condensing molecule with all other molecules within the cutoff radius of 0.85 nm (see simulation details above, and Figure 1b for an example) and refer to it simply as “interaction energy”  $E$ .

**2.2. Re-Analysis of Environmental Molecular Beam Data Using Molecular Flux Modeling.** To complement the molecular perspective rising from the MD simulations and discuss it in the context of observables linked to accommodation, we use molecular flux modeling based on thermodynamic and kinetic theories to re-analyze relatively recent experimental data on the accommodation coefficient of water into a bulk ice phase obtained with an environmental molecular beam (EMB) apparatus.<sup>27</sup> The experiment devised by Kong et al. is based on the measurement of D<sub>2</sub>O molecular intensities originating from the surface of a H<sub>2</sub>O-ice slab subjected to previous D<sub>2</sub>O deposition. Here, we evaluate the observed D<sub>2</sub>O desorption recorded by the EMB apparatus to investigate the sensitivity of the observed molecular fluxes to potential non-accommodation events. To do this, we use two molecular flux modeling schemes that approximate the evaporation from a disordered interface assumed to consist of an ideal mixture of D<sub>2</sub>O and H<sub>2</sub>O: one accounting for evaporative losses only and one that additionally accounts for bulk accommodation events.

The molecular flux models are predicated upon proportionality between the detected D<sub>2</sub>O flux from the sample surface and the surface layer D<sub>2</sub>O concentration  $I \propto N_{D_2O}$ . In the experimental setup, D<sub>2</sub>O is first deposited onto an initially D<sub>2</sub>O-free sample by the molecular beam at rate  $\Gamma$  for a short time interval  $[t_1, t_2]$ . After this, the number concentration  $N_{D_2O}$  in the surface layer decreases as the molecules simultaneously evaporate from the surface or accommodate into the bulk ice. The change rate of  $N_{D_2O}$  can thus be written as

$$\frac{dN_{D_2O}}{dt} = \begin{cases} 0; & t < t_1 \\ \Gamma - k_{\text{sum}}N_{D_2O}; & t_1 < t < t_2 \\ k_{\text{sum}}N_{D_2O}; & t_2 < t \end{cases} \quad (2.2)$$

where the D<sub>2</sub>O deposition takes place for times  $t_1 < t < t_2$  and  $k_{\text{sum}}$  is the sum of the evaporation and accommodation rate constants  $k_{\text{sum}} = k_e + k_a$ . Integration of eq 2.2 yields the time-dependent surface concentration

$$N_{D_2O} = \begin{cases} 0; & t < t_1 \\ \frac{\Gamma}{k_{\text{sum}}}[1 - e^{-k_{\text{sum}}(t-t_1)}]; & t_1 < t < t_2 \\ N_0 e^{-k_{\text{sum}}(t-t_2)}; & t_2 < t \end{cases} \quad (2.3)$$

where  $N_0 = \frac{\Gamma}{k_{\text{sum}}}[1 - e^{-k_{\text{sum}}(t_2-t_1)}]$  is the surface concentration at  $t = t_2$  when the beam is switched off. The detected intensity is connected to  $N_{D_2O}$  through the evaporation flux as

$$I(t) = A \times B \times k_e N_{D_2O}(t) \quad (2.4)$$

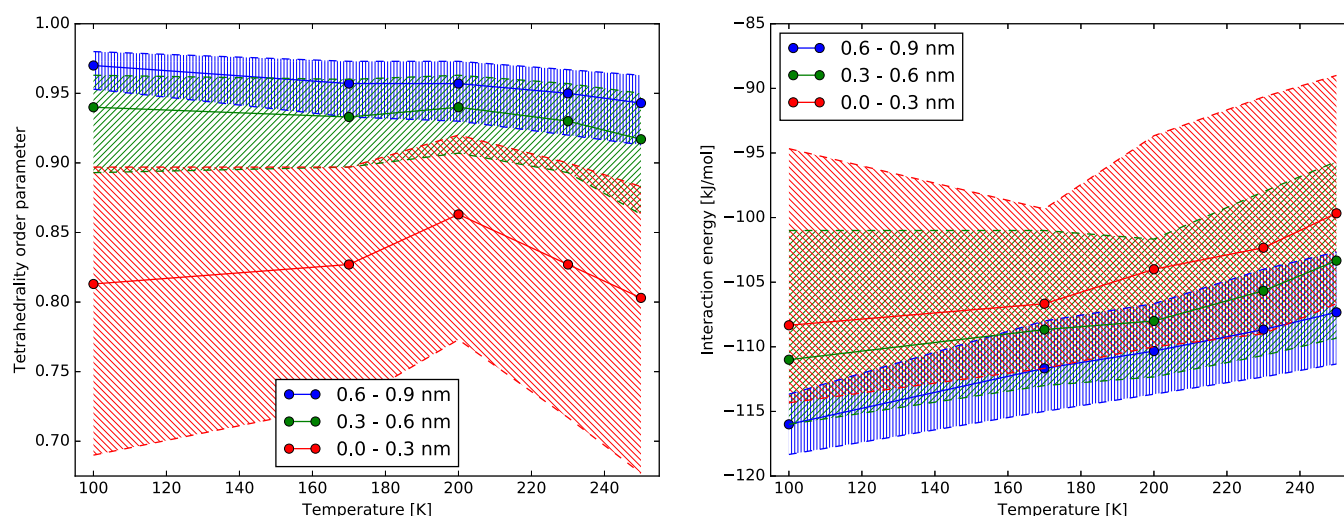


**Figure 3.** Medians of the distributions of tetrahedrality parameters (left) and interaction energies (right) as functions of temperature for the three topmost 3 Å layers. The hatched areas depict the width of the distributions as 25–75 quartiles.

where the prefactor  $B$  is determined from the known experimental settings and includes, e.g., the slab-to-detector transmission efficiency (see the [Supporting Information](#)),  $k_e$  is the evaporation rate constant, and  $A$  is a fitting parameter. Here, we use the standard Knudsen evaporation rate for  $k_e$  as

$$k_e = X \frac{\langle v \rangle C_S}{4} \quad (2.5)$$

where  $\langle v \rangle$  is the mean thermal velocity of gas-phase  $D_2O$  molecules,  $C_S$  is the saturation vapor concentration over the surface, and  $X$  is a parameter accounting for unit conversions and mixing with  $H_2O$  molecules (see the [Supporting Information](#)). This approach is chosen to prevent introducing additional experimental uncertainties from Arrhenius-type evaporation rates derived from fits to the measurement data (see Figure S**b** in Kong et al.<sup>27</sup>). Unlike in the previous studies, we do not need to fit the thermal evaporation rate but can predict it “bottom-up” if the saturation vapor pressure of  $D_2O$  and the thickness of the disordered layer as a function of temperature can be estimated. After removing the average background signal,  $I_n(t)$  is fit to data recorded at 12 temperatures spanning 170–200 K using two approaches. First, we apply an evaporation-only model in which  $k_{\text{sum}} = k_e$  and a single parameter  $A$  is fit; second, an evaporation and bulk accommodation model is used, in which  $k_{\text{sum}} = k_e + k_\alpha$  and both  $A$  and the bulk accommodation rate  $k_\alpha$  are fit. These fits are used to assess how well the data can be described by such models, and how reliably the accommodation rate constant  $k_\alpha$  can be constrained from such data.

### 3. RESULTS AND DISCUSSION

**3.1. Molecular Definition of Surface and Bulk Accommodation from MD Simulations.** A condensing gas-phase molecule can be considered “accommodated” when its physical state is not distinguishable from that of surface (in case of  $\alpha_s$ ) or bulk (in case of  $\alpha_b$ )-phase molecules. This axiom is used here to develop criteria for the accommodated states in the disordered surface phase and in the bulk ice. First, we examine the ice slab (excluding the condensing molecule) to characterize the tetrahedrality parameter  $q$  and the interaction energy  $E$  (Section 2.1) of molecules present in the surface layer

and in the bulk ice. We use these data to define the accommodated (AC) states and to determine the fraction of condensing molecules that enter the so-defined AC subspaces.

Figure 2 shows the distributions of the tetrahedrality parameter and the interaction energy of the slab molecules at different distances from the instantaneous interface. As expected, the distributions display slightly increasing maxima upon decreasing temperature and small shifts toward higher tetrahedrality parameters and more negative interaction energies. At the same time, they overlap significantly for all layers and all temperatures, except for a narrow binning of 0.5 Å in the topmost layers (insets in Figure 2), where the order parameter reflects the disorder at the interface and the molecules are not able to establish all hydrogen-bond configurations that would be possible in the bulk due to an anisotropic local environment. These results are consistent with those obtained by Gladich et al.<sup>52</sup> who used the same parameter to characterize the surface layer and investigated the anisotropic surface self-diffusion within the quasi-liquid layer at different temperatures using a six-site model of water.

Figure 3 shows the medians of the  $q$  and  $E$  distributions (Figure 2) at different temperatures together with the spread indicating the 25th and 75th quartiles for the three topmost layers of 3 Å thickness. The distribution of tetrahedrality parameters in the topmost layer differs slightly from those of the other layers, while the interaction energy distributions overlap for all layers. This observation is valid almost independent of temperature. These results indicate that the key parameter differentiating the surface- and bulk-accommodated states is the tetrahedrality parameter, while in terms of the interaction energy these two states are almost indistinguishable from each other.

Based on the above results, it is clear that the criteria for both surface and bulk accommodation must be temperature-dependent but also that defining the accommodated states is not unambiguous even for the slab molecules. We define AC criteria for both the surface and the bulk-accommodated states, given by the medians of the distributions of  $q$  and  $E$  of the topmost and the third layer (0.6–0.9 nm below the interface), respectively, as presented in Figure 3. The specific values obtained are listed in Table 1 for all temperatures. These

**Table 1.** Definition of “Surface-Accommodated” and “Bulk-Accommodated” Subspaces Using the Medians of  $q$  and  $E$  Distributions<sup>a</sup>

$T$ [K]	Surface ( $-3 \text{ \AA} < d \leq 0 \text{ \AA}$ ) AC sub-space (medians)		Bulk ( $-9 \text{ \AA} < d \leq 6 \text{ \AA}$ ) AC sub-space (medians)	
	$q$	$E$ [kJ/mol]	$q$	$E$ [kJ/mol]
100	0.813	-108.3	0.970	-116.0
170	0.827	-106.7	0.957	-111.7
200	0.863	-104.0	0.957	-110.3
230	0.827	-102.3	0.950	-108.7
250	0.803	-99.7	0.943	-107.3

<sup>a</sup>The subspace definition is based on a subdivision into  $3 \text{ \AA}$  layers (about one molecular diameter) parallel to the instantaneous interface.

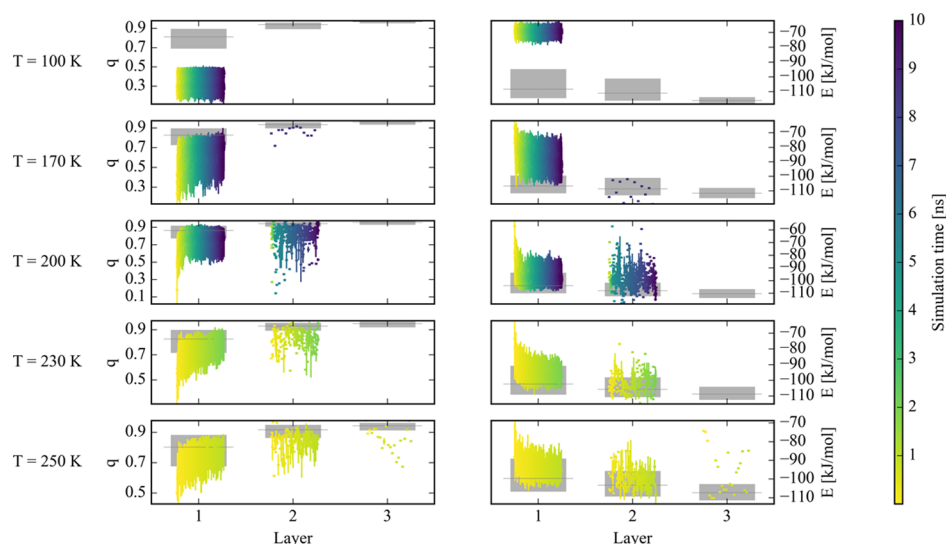


**Figure 4.** Characteristic values of interaction energy and tetrahedrality parameter distributions of the slab (gray bars) and condensed molecules (colored lines). The bars indicate the 25th–75th percentiles and the median is indicated with a thin line; condensing molecules’ distributions are obtained as median and 25th–75th percentiles of up to 100 molecules at times encoded in their color. Absence of condensing molecules’ distribution lines at low temperatures and in the lower layers indicates that no condensing molecules have diffused to the layer in question within the respective simulation time.

values can be discussed in light of the desorption energy  $E_{\text{des}} = 42 \pm 8 \text{ kJ/mol}$  and the energy related to the incorporation of water molecules into the ice structure  $E_1 = 6 \pm 5 \text{ kJ/mol}$  (interpreted here as the energy associated with the bulk accommodation) reported by Kong et al. based on adsorption-model fits to the same data as discussed in Section 3.3. Specifically, it is interesting that the difference in  $E$  between the surface and the bulk-accommodated states is  $5\text{--}8 \text{ kJ/mol}$  and thus comparable in magnitude to the  $E_1$  value by Kong et al. while being significantly smaller than the desorption energy.

It is important to note that while the statistics over a large number of molecules give rise to the average properties of the slab layers, the individual molecules are subjected to pronounced thermal fluctuations—the magnitude of which increases with temperature. A bulk molecule can be in an AC state with fluctuations into non-AC states and vice versa. The exchange frequencies between the AC (see Table 1) and non-AC states lie in the range of  $0 \leq f_{\text{ex}} \leq 30 \text{ ns}^{-1}$  for all temperatures, with a tendency of higher frequencies in the center of the slab and lower frequencies in the surface layer (see Supporting Information). We interpret this finding as a result of stronger bonds at crystal sites than at the surface, in analogy to the frequency of a harmonic oscillator depending on the force constant. This picture also explains the trend in the

AC state definition with temperature since the mean square displacement of molecules about crystal sites due to thermal motion is directly proportional to temperature, assuming a harmonic potential. Enhanced spatial fluctuations would in turn cause fluctuations in interaction energy and tetrahedrality parameter that cause fluctuations into and out of a given AC subspace. Closer to the interface and at higher temperatures, the approximation of harmonic potentials naturally cannot be expected to hold while the qualitative considerations are unaffected.

### 3.2. Kinetics of Condensing Molecules and Time Scales Related to Accommodation.

Let us now discuss the kinetics and time scales of the accommodation process of a condensing vapor-phase molecule implementing the above criteria, as this will be critical for linking the theoretical findings to experimental data. Furthermore, the time scales associated with the accommodation phenomena are expected to be highly dependent on temperature and hence important when discussing the potential explanations to the observed temperature trends.

Figure 4 shows a comparison of the  $q$  and  $E$  distributions of the condensing molecules throughout the simulation time as compared with those of the slab molecules (see Figure 2) as a function of temperature. The distributions of slab molecules

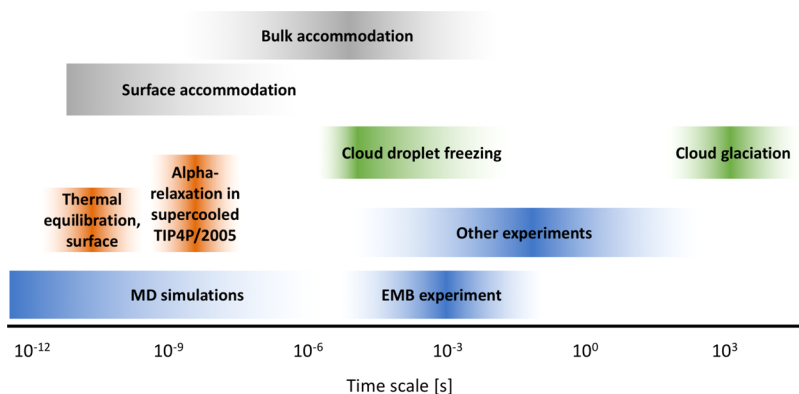


**Figure 5.** Schematic illustrating the time scales of different methods and phenomena of interest in the context of accommodation processes: typical time scales of MD simulations and EMB experiments by Kong et al. considered here, estimates for time scales of surface and bulk accommodation processes, surface relaxation time scales,<sup>16</sup> structural relaxation time scale in simulations of supercooled bulk water,<sup>54</sup> and typical time scales of associated cloud-microphysical processes.<sup>55</sup>

(gray) are statistics over the whole trajectory, represented by mean and quartiles, while the distributions of the condensed molecules represent statistics over up to 100 simulations for each time bin of 10 ps. Every colored line thus represents the distributions of tetrahedrality parameter and interaction energy, respectively, with its color encoding the time bin along the trajectory. It can be seen that while the distributions overlap for temperatures  $T > 100$  K, the condensed molecules have generally lower tetrahedrality parameters and less negative interaction energies than the slab molecules in the same layer, with the distributions of the condensed molecules shifting toward those of the bulk molecules over time. Furthermore, it is notable that the condensing molecules do not diffuse beyond the first layer for  $T = 100$  K within our simulation time of 10 ns, while they distribute over first, second, and third layers for  $T = 250$  K even within shorter simulation times of 1 ns. These results suggest that the time scales of both surface and bulk accommodation are indeed highly dependent on temperature. Once the condensing molecule adsorbs onto the disordered surface layer, it will thermally equilibrate with its nearest neighbors within some 10 ps,<sup>16</sup> and subsequently its interaction energy and tetrahedrality parameter will gradually become indistinguishable from the slab molecules. Defined this way, the surface accommodation process is estimated to happen within time scales of roughly 1 ns ( $T = 250, 230$  K), 10 ns ( $T = 200$  K), 45 ns ( $T = 170$  K), and 250 ns ( $T = 100$  K), based on the decay of the time correlation functions of  $q$  and  $E$  (see Figure S2 and Table S5).

Uptake into the disordered interface thus plays a decisive role being the first step in the accommodation process: the subsequent bulk accommodation of the initially labeled molecule into the bulk crystal becomes equivalent to the concept of equilibrium exchange processes of slab molecules between the bulk crystal and its disordered surface layer. Based on literature values of ice growth rates in Xu et al.,<sup>53</sup> the time scale of the bulk accommodation from the surface layer is hence expected to vary considerably, ranging from nanoseconds to seconds between 126 and 262 K, showing a minimum around 250 K.<sup>53</sup> These estimates are also in line with our simulations, where some molecules reached the accommodated state within 10 ns while others did not, and the median properties of the condensing molecules were closest to the slab values at 250 K (see Figure 4). Specifically, the condensing molecules are observed not to diffuse beyond the

topmost layer for all temperatures but rather stay at the interface for lower temperatures beyond time scales covered by the simulations presented here. Simulation studies of equilibration kinetics would require ergodic sampling and thus much longer simulation times of the order of microseconds. Furthermore, these expected accommodation time scales are all considerably shorter than the microsecond time scales probed by the EMB experiment discussed in detail below. A schematic overview of the different time scales is presented in Figure 5.

To illustrate the accommodation process in more detail, Figure 1 shows typical example snapshots from a simulation trajectory at 200 K visualizing a gas-phase molecule condensing onto the ice surface (Figure 1a) and the interaction energy and the tetrahedrality parameter of the molecule as a function of time (Figure 1b). The instantaneous interface is indicated in blue and the condensing molecule is followed while penetrating this interface. Initial adsorption onto the surface layer, indicated by a drop in interaction energy to around  $-50$  kJ/mol, takes place within the first few ps of the simulation. This is followed by reorientation movements of the condensing molecule associated with fluctuations in interaction energy and tetrahedrality parameter. At about 182 ps, there is a transition into a lower energy, i.e., a stronger binding, state at an energy fluctuation of about  $-90$  to  $-100$  kJ/mol. We attribute the different interaction energy states to different hydrogen-bonded (H-bonded) configurations. The snapshot at  $t = 182$  ps shows the condensing molecule having penetrated the instantaneous surface, accompanied by an exchange process with a molecule from the surface layer, H-bonding to the condensed molecule. The resulting near-tetrahedral coordination of the condensed molecule gives rise to a temporarily very high tetrahedrality parameter and a very negative interaction energy, as seen in Figure 1b.

To further examine the potential bulk accommodation in our simulations, results from a first passage time (FPT) analysis are shown in Figure 6, where the cumulative fraction of simulations exhibiting a surface (Figure 6a) or bulk (Figure 6b) accommodation event (following the criteria in Table 1) for the first time is presented as a function of time for each temperature. While the cumulative FPT distributions for all temperatures change toward a lower fraction of molecules being accommodated in the bulk-like states as compared with the surface-like states, this change is observed to be most

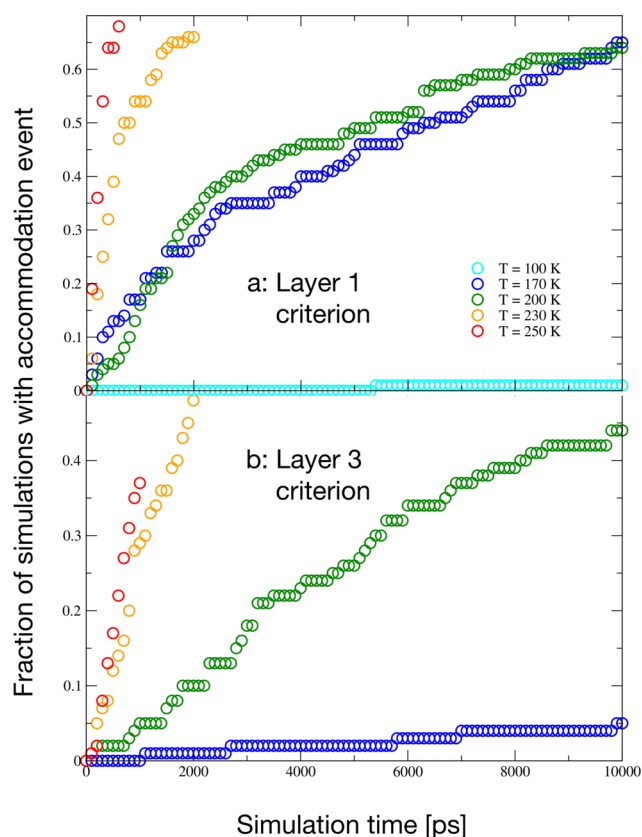


**Figure 6.** First passage time (FPT) analysis. Fraction of 100 simulations with a condensing vapor-phase molecule that exhibits an accommodation event as a function of time (100 ps time bins). An accommodation event is identified when the condensing molecule enters the accommodated space defined for the respective temperature for the first time. (a) AC criteria found from the medians of interaction energy and tetrahedrality parameter in layer 1 ( $-0.3 \text{ nm} < d \leq 0.0 \text{ nm}$ ); (b) corresponding criteria found in layer 3 ( $-0.6 \text{ nm} \leq d < -0.9 \text{ nm}$ ), see Table 1.

pronounced for  $T = 170 \text{ K}$ . Simulations at  $T = 100 \text{ K}$  were not run long enough to resolve more accommodation events. We emphasize that the FPT accommodation rate, corresponding to the slope of the FPT distributions, seems to undergo a rather dramatic change between  $T = 170$  and  $200 \text{ K}$  when the criteria are changed from weaker to stronger. This observation indicates that, within our simulation time, there is a significant amount of transitions into accommodated states in both definitions around  $200 \text{ K}$  and above, while the stronger accommodation criterion is met far less frequently for lower temperatures. This can be understood in terms of a slowdown of the dynamics with decreasing temperature, which also makes the exchange processes less likely, as discussed above. These results further emphasize the strong temperature dependence of the accommodation processes (see also Table S1 and Figure 4): while the time scales of surface and bulk accommodation are similar for temperatures between  $200$  and  $250 \text{ K}$ , they diverge at lower temperatures where the bulk processes become drastically slower. Both time scales generally shorten with increasing temperature in the temperature range probed here ( $100\text{--}250 \text{ K}$ ).

The frequency of exchange between accommodated and non-accommodated states discussed above can further be compared to the FPT accommodation rate. While the exchange frequencies are found in the range of  $0 \leq f_{\text{ex}} \leq 30$

$\text{ns}^{-1}$ , the FPT accommodation rates cover a wider interval of roughly  $0 \leq f_{\text{FPT}} \leq 130 \text{ ns}^{-1}$ , with good agreement at low temperatures where the frequencies are of the orders  $0.1\text{--}10 \text{ ns}^{-1}$  (see also Supporting Information).

Along the trajectories of the condensing molecules, the tetrahedrality parameter  $q$  is roughly anticorrelated with the interaction energy  $E$  in the condensed phase (see Figure 1 for  $200 \text{ K}$ ). Generally,  $q$  increases with more negative distances together with increasingly negative  $E$ , indicating the structural order to increase the further the molecule penetrates the surface layer toward the bulk. As a summary, tetrahedrality parameter, interaction energy, and the distance to the instantaneous interface are not strictly independent: generally, molecules with the strongest binding energy tend to correlate with the highest values of  $q$  and lie deepest down in the surface layer. The choice of these parameters for defining the accommodated states within the surface and the bulk is, however, justified e.g., by the distinctly different behavior of the bulk vs surface visible in the tetrahedrality parameter but not in the interaction energy (see Figure 3).

**3.3. Interpretation of the EMB Data by Evaporation–Accommodation Modeling.** Our sensitivity analysis utilizing one- and two-parameter fits (see Section 2 and the Supporting Information), respectively, clearly shows that evaporation alone cannot explain the depletion of  $\text{D}_2\text{O}$  at the ice surface, particularly for temperatures below  $190 \text{ K}$ , in agreement with earlier results by Kong et al. The evaporation rate is, on the other hand, a major source of uncertainty (see Supporting Information), due to uncertainties in the vapor pressure parameterizations. We find that an evaporation rate calculated from Knudsen theory with the vapor pressure of  $\text{D}_2\text{O}$  ice as obtained by Matsuo et al.<sup>56</sup> can fit the data to the same accuracy as the Arrhenius-type evaporation rate employed by Kong et al., whose fit yields a desorption activation energy of  $42 \pm 9 \text{ kJ/mol}$ <sup>27</sup> (cf. Supporting Information).

Reproducing the results obtained earlier, we investigated the theoretical maximum fraction of molecules that can evaporate from the surface after deposition within a certain time interval, without any accommodation taken into account. Figure 7 shows the evaporated fraction  $F_e(T, t_{\text{end}})$  as a function of temperature  $T$  and elapsed time after deposition  $t_{\text{end}}$ . This analysis suggests that an experimental time window of  $60 \text{ ms}$  might be insufficient and could potentially lead to an artificially high value of  $\alpha$  at low temperatures, a concern raised earlier by Kong et al. This suggests that the experimental data is possibly insufficient to conclusively constrain the bulk accommodation process. Furthermore, as both evaporation and accommodation processes are temperature-dependent, it is challenging to disentangle their effects on the observed signal. For instance, the fact that more  $\text{D}_2\text{O}$  desorbed from the surface is detected at higher temperatures may be due to increased, highly uncertain, evaporation rate, instead of reflecting reduced bulk accommodation. These results suggest that techniques that are able to directly characterize the surface states would be favorable compared to indirect assessments of surface processes, and that adaptable sampling time windows are beneficial when measurements are performed at different temperatures. Further development of the EMB technique toward longer measurement time intervals and improved signal-to-noise ratio, on the other hand, is a promising alternative as this allows the direct observation of the sorption kinetics.

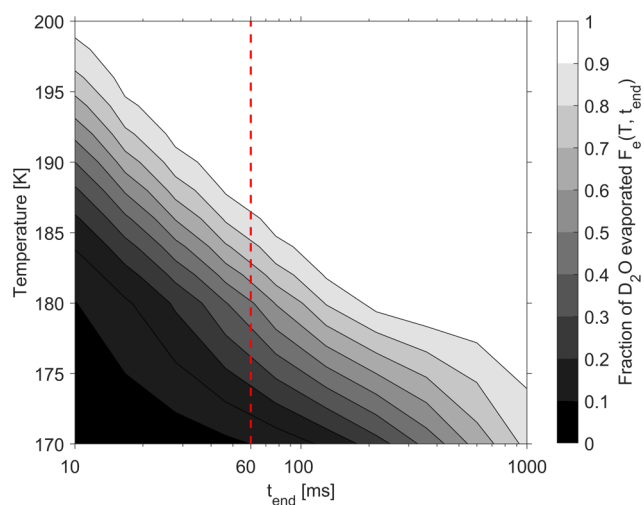


**Figure 7.** Contour plot of the theoretical fraction of initially deposited  $D_2O$  molecules  $F_e(T, t_{end})$  that have evaporated at temperature  $T$  after time  $t_{end}$ , disregarding accommodation and using the vapor pressure of  $D_2O$  from ref 56. The dashed red line marks the observation time window in the EMB experiment by Kong et al.

#### 4. CONCLUSIONS

In the present study, we set out to characterize the accommodation process using molecular dynamics simulations. The simulations suggest that the definition of the accommodated state plays a decisive role in characterizing and interpreting the accommodation of water vapor on ice due to the presence of the disordered layer on top of ice surfaces. Molecules within this layer undergo fluctuations between more ordered, ice-like states and less ordered surface states. Therefore, even if a condensing vapor-phase molecule is not built into the bulk ice lattice immediately after impinging the surface, it can be considered accommodated to the surface as soon as its energetics and orientational order cannot be distinguished from those of the surrounding surface molecules at equilibrium. Recognizing the surface layer of ice to be disordered to an extent depending on the temperature difference to the melting temperature, we investigate distributions of the molecular tetrahedrality parameter and the interaction energy as functions of depth below the instantaneous interface and as functions of temperature. Based on these distributions, we define the space of accommodated states. We emphasize that even under equilibrium conditions, molecules that are part of the simulated ice slab fluctuate into and out of these so-defined accommodated states.

The interaction energy is naturally dominated by the hydrogen-bond state of the molecule considered. From our analysis of energy distributions, the differences associated with the transition between the surface layer and the bulk crystal widely overlap, and the associated energy change is thus very difficult to constrain from measurements where also evaporation (with an uncertain evaporation rate) takes place. While it is evident that the experimental data by Kong et al. cannot be described by evaporation alone, bulk accommodation is difficult to reliably be dissected from the data as the signal is heavily influenced by the uncertainty in the evaporation rate.

We find here that the distribution of molecular interaction energies does not provide a sensitive measure in the context of accommodation while the tetrahedrality parameter is a much

more suitable means to distinguish surface and bulk states. This result indicates that experiments probing bulk accommodation from the surface layer should preferably be able to resolve structural changes on molecular scales.

Having characterized the slab molecules, we follow the evolution of individual molecules condensing onto the surface while their properties relax toward those of the slab molecules. The above analysis demonstrates a strong temperature dependence of the surface and bulk accommodation kinetics: the time correlation functions yield relaxation times for surface layer accommodation of the order of 1 ns at 250 K and 250 ns at 100 K, while literature data on ice crystal growth rates suggests bulk accommodation time scales ranging from nanoseconds to seconds in a similar temperature range.<sup>53</sup> This highlights the need for being able to adjust the time window probed in any experiments targeted to observe the kinetics of water vapor accommodation as a function of temperature.

Our first passage time analysis shows a rather pronounced drop in the accommodation rate below  $T = 200$  K and on the time scales resolved in this study, when results obtained with the stronger criteria, deduced from bulk molecular states, are compared to those obtained with the weaker criteria that were deduced from molecular states in the surface layer. Thus, we argue that depositional ice growth can be thought of as a two-step process, with an initial adsorption to the disordered surface layer and subsequent accommodation into the bulk crystal on longer time scales.

We note that the concept of accommodation of vapor-phase molecules into an ice crystal is tightly interconnected to crystal growth rather than to equilibrium dynamics. Measurements of ice crystal growth show that the growth rate at atmospherically relevant conditions is orders of magnitudes faster than any net condensation flux for a wide temperature range (100–280 K).<sup>3</sup> This means that a possible energy barrier to accommodation to the ice lattice (if any) is so small that it is not expected to play any role in the atmospheric context. This makes the uptake of condensing molecules onto the surface the rate-limiting process. In this case, the relevant parameter characterizing accommodation is the sticking coefficient of vapor molecules colliding with the surface, for which numerous simulation studies have indicated a value of unity for the liquid water surface.<sup>7,14,57</sup> At temperatures close to the melting temperature, we speculate that this value should not be different for the premelting layer of ice than for the surface of the liquid and thus expect a value of unity for the surface accommodation also in this case.

#### ■ ASSOCIATED CONTENT

##### SI Supporting Information

The Supporting Information is available free of charge at <https://pubs.acs.org/doi/10.1021/acs.jpca.0c09357>.

Evaluation of the flux models for the re-analysis of EMB data, details on the interaction energy and tetrahedrality parameter distributions from MD simulations, interaction energy and tetrahedrality parameter time correlation functions of condensing molecules, and an analysis of exchange frequencies between accommodated states (PDF)

## ■ AUTHOR INFORMATION

## Corresponding Authors

**Daniel Schlesinger** – Department of Environmental Science (ACES), Stockholm University, SE-106 91 Stockholm, Sweden; Bolin Centre for Climate Research, Stockholm University, SE-106 91 Stockholm, Sweden; [orcid.org/0000-0001-7889-1964](https://orcid.org/0000-0001-7889-1964); Email: [Daniel.Schlesinger@aces.su.se](mailto:Daniel.Schlesinger@aces.su.se)

**Ilona Riipinen** – Department of Environmental Science (ACES), Stockholm University, SE-106 91 Stockholm, Sweden; Bolin Centre for Climate Research, Stockholm University, SE-106 91 Stockholm, Sweden; [orcid.org/0000-0001-9085-2319](https://orcid.org/0000-0001-9085-2319); Email: [Ilona.Riipinen@aces.su.se](mailto:Ilona.Riipinen@aces.su.se)

## Authors

**Samuel J. Lowe** – Department of Environmental Science (ACES), Stockholm University, SE-106 91 Stockholm, Sweden; Bolin Centre for Climate Research, Stockholm University, SE-106 91 Stockholm, Sweden

**Tinja Olenius** – Department of Environmental Science (ACES), Stockholm University, SE-106 91 Stockholm, Sweden; Bolin Centre for Climate Research, Stockholm University, SE-106 91 Stockholm, Sweden

**Xiangrui Kong** – Department of Chemistry and Molecular Biology, Atmospheric Science, University of Gothenburg, SE-412 96 Gothenburg, Sweden

**Jan B. C. Pettersson** – Department of Chemistry and Molecular Biology, Atmospheric Science, University of Gothenburg, SE-412 96 Gothenburg, Sweden; [orcid.org/0000-0001-8420-6126](https://orcid.org/0000-0001-8420-6126)

Complete contact information is available at: <https://pubs.acs.org/10.1021/acs.jpca.0c09357>

## Notes

The authors declare no competing financial interest.

<sup>||</sup>Present Address: (T.O.) Research Department, Air Quality Research Unit, Swedish Meteorological and Hydrological Institute (SMHI), SE-601 76 Norrköping, Sweden.

## ■ ACKNOWLEDGMENTS

The authors gratefully acknowledge funding through the K&A Wallenberg Foundation (Project AtmoRemove 2015.0162), and the European Union's Horizon 2020 Research and Innovation Programme under Grant Agreement No. 865799 (ERC Consolidator Grant INTEGRATE) and 821205 (FORCeS). The simulations were performed on resources provided by the Swedish National Infrastructure for Computing (SNIC) at the National Supercomputer Centre (NSC) and the High Performance Computing Centre North (HPC2N). D.S. thanks Evgeni Zapadinski for useful comments on an early version of the manuscript. T.O. thanks the ÅForsk Foundation (Project 18-334) for financial support.

## ■ REFERENCES

- (1) Pruppacher, H. R.; Klett, J. D. *Microphysics of Clouds and Precipitation*, 2nd ed.; Springer: Netherlands, 2010.
- (2) Lamb, D.; Verlinde, J. *Physics and Chemistry of Clouds*; Cambridge University Press, 2011.
- (3) Seinfeld, J. H.; Pandis, S. N. *Atmospheric Chemistry and Physics: From Air Pollution to Climate Change*; John Wiley & Sons, 2016.
- (4) Fuchs, N. A.; Sutugin, A. G. *Highly Dispersed Aerosols*; Ann Arbor Science, 1970.

(5) Kolb, C. E.; Cox, R. A.; Abbatt, J. P. D.; Ammann, M.; Davis, E. J.; Donaldson, D. J.; Garrett, B. C.; George, C.; Griffiths, P. T.; Hanson, D. R.; et al. An Overview of Current Issues in the Uptake of Atmospheric Trace Gases by Aerosols and Clouds. *Atmos. Chem. Phys.* **2010**, *10*, 10561–10605.

(6) Vehkamäki, H.; Riipinen, I. Thermodynamics and Kinetics of Atmospheric Aerosol Particle Formation and Growth. *Chem. Soc. Rev.* **2012**, *41*, 5160–5173.

(7) Varilly, P.; Chandler, D. Water Evaporation: A Transition Path Sampling Study. *J. Phys. Chem. B* **2013**, *117*, 1419–1428.

(8) Lohmann, U.; Lüönd, F.; Mahrt, F. *An Introduction to Clouds: From the Microscale to Climate*; Cambridge University Press, 2016.

(9) Sinha, A.; Saleh, R.; Robinson, E. S.; Ahern, A. T.; Tkacik, D. S.; Presto, A. A.; Sullivan, R. C.; Robinson, A. L.; Donahue, N. M. Mass Accommodation Coefficients of Fresh and Aged Biomass-Burning Emissions. *Aerosol Sci. Technol.* **2018**, *52*, 300–309.

(10) Liu, X.; Day, D. A.; Krechmer, J. E.; Brown, W.; Peng, Z.; Ziemann, P. J.; Jimenez, J. L. Direct Measurements of Semi-Volatile Organic Compound Dynamics Show near-Unity Mass Accommodation Coefficients for Diverse Aerosols. *Commun. Chem.* **2019**, *2*, No. 98.

(11) Kulmala, M.; Wagner, P. E. Mass Accommodation and Uptake Coefficients—a Quantitative Comparison. *J. Aerosol Sci.* **2001**, *32*, 833–841.

(12) Hienola, J.; Kulmala, M.; Laaksonen, A. Condensation and Evaporation of Water Vapor in Mixed Aerosols of Liquid Droplets and Ice: Numerical Comparison of Growth Rate Expressions. *J. Aerosol Sci.* **2001**, *32*, 351–374.

(13) Pöschl, U.; Rudich, Y.; Ammann, M. Kinetic Model Framework for Aerosol and Cloud Surface Chemistry and Gas-Particle Interactions - Part I: General Equations, Parameters, and Terminology. *Atmos. Chem. Phys.* **2007**, *7*, 5989–6023.

(14) Julin, J.; Shiraiwa, M.; Miles, R. E.; Reid, J. P.; Pöschl, U.; Riipinen, I. Mass Accommodation of Water: Bridging the Gap between Molecular Dynamics Simulations and Kinetic Condensation Models. *J. Phys. Chem. A* **2013**, *117*, 410–420.

(15) Bartels-Rausch, T.; Jacobi, H.-W.; Kahan, T. F.; Thomas, J. L.; Thomson, E. S.; Abbatt, J. P.; Ammann, M.; Blackford, J. R.; Bluhm, H.; Boxe, C.; et al. A Review of Air–Ice Chemical and Physical Interactions (AICI): Liquids, Quasi-Liquids, and Solids in Snow. *Atmos. Chem. Phys.* **2014**, *14*, 1587–1633.

(16) Neshyba, S.; Nugent, E.; Roeselová, M.; Jungwirth, P. Molecular Dynamics Study of Ice–Vapor Interactions via the Quasi-Liquid Layer. *J. Phys. Chem. C* **2009**, *113*, 4597–4604.

(17) Miles, R. E. H.; Reid, J. P.; Riipinen, I. Comparison of Approaches for Measuring the Mass Accommodation Coefficient for the Condensation of Water and Sensitivities to Uncertainties in Thermophysical Properties. *J. Phys. Chem. A* **2012**, *116*, 10810–10825.

(18) Winkler, P. M.; Vrtala, A.; Wagner, P. E.; Kulmala, M.; Lehtinen, K. E. J.; Vesala, T. Mass and Thermal Accommodation during Gas-Liquid Condensation of Water. *Phys. Rev. Lett.* **2004**, *93*, No. 075701.

(19) Winkler, P. M.; Vrtala, A.; Rudolf, R.; Wagner, P. E.; Riipinen, I.; Vesala, T.; Lehtinen, K. E. J.; Viisanen, Y.; Kulmala, M. Condensation of Water Vapor: Experimental Determination of Mass and Thermal Accommodation Coefficients. *J. Geophys. Res.* **2006**, *111*, No. D19202.

(20) Dash, J.; Rempel, A.; Wettlaufer, J. The Physics of Premelted Ice and Its Geophysical Consequences. *Rev. Mod. Phys.* **2006**, *78*, No. 695.

(21) Slater, B.; Michaelides, A. Surface Premelting of Water Ice. *Nat. Rev. Chem.* **2019**, *3*, 172–188.

(22) Conde, M.; Vega, C.; Patrykiewicz, A. The Thickness of a Liquid Layer on the Free Surface of Ice as Obtained from Computer Simulation. *J. Chem. Phys.* **2008**, *129*, No. 014702.

(23) Limmer, D. T.; Chandler, D. Premelting, Fluctuations, and Coarse-Graining of Water-Ice Interfaces. *J. Chem. Phys.* **2014**, *141*, No. 18C505.

- (24) Koros, R. M.; Deckers, J. M.; Andres, R. P.; Boudart, M. The Sticking Probability of Water on Ice. *Chem. Eng. Sci.* **1966**, *21*, 941–950.
- (25) Bryson, C. E.; Cazcarra, V.; Levenson, L. L. Condensation Coefficient Measurements of H<sub>2</sub>O, N<sub>2</sub>O, and CO<sub>2</sub>. *J. Vac. Sci. Technol.* **1974**, *11*, 411–416.
- (26) Brown, D. E.; George, S. M.; Huang, C.; Wong, E. K. L.; Rider, K. B.; Smith, R. S.; Kay, B. D. H<sub>2</sub>O Condensation Coefficient and Refractive Index for Vapor-Deposited Ice from Molecular Beam and Optical Interference Measurements. *J. Phys. Chem. A* **1996**, *100*, 4988–4995.
- (27) Kong, X.; Papagiannakopoulos, P.; Thomson, E. S.; Markovic, N.; Pettersson, J. B. Water Accommodation and Desorption Kinetics on Ice. *J. Phys. Chem. A* **2014**, *118*, 3973–3979.
- (28) Tolbert, M. A.; Middlebrook, A. M. Fourier Transform Infrared Studies of Model Polar Stratospheric Cloud Surfaces: Growth and Evaporation of Ice and Nitric Acid/Ice. *J. Geophys. Res.* **1990**, *95*, 22423–22431.
- (29) Haynes, D. R.; Tro, N. J.; George, S. M. Condensation and Evaporation of Water on Ice Surfaces. *J. Phys. Chem. B* **1992**, *96*, 8502–8509.
- (30) Magee, N.; Moyle, A. M.; Lamb, D. Experimental Determination of the Deposition Coefficient of Small Cirrus-like Ice Crystals near –50 °C. *Geophys. Res. Lett.* **2006**, *33*, No. L17813.
- (31) Kramers, H.; Stermerding, S. The Sublimation of Ice in Vacuum. *Appl. Sci. Res.* **1951**, *3*, 73–82.
- (32) Leu, M.-T. Heterogeneous Reactions of N<sub>2</sub>O<sub>5</sub> with H<sub>2</sub>O and HCl on Ice Surfaces: Implications for Antarctic Ozone Depletion. *Geophys. Res. Lett.* **1988**, *15*, 851–854.
- (33) Chaix, L.; Allanic, A.; Rossi, M. J. Heterogeneous Chemistry of HOBr on Different Types of Ice and on Ice Doped with HCl, HBr, and HNO<sub>3</sub> at 175 K < T < 215 K. *J. Phys. Chem. A* **2000**, *104*, 7268–7277.
- (34) Fluckiger, B.; Rossi, M. J. Common Precursor Mechanism for the Heterogeneous Reaction of D<sub>2</sub>O, HCl, HBr, and HOBr with Water Ice in the Range 170–230 K: Mass Accommodation Coefficients on Ice. *J. Phys. Chem. A* **2003**, *107*, 4103–4115.
- (35) Delval, C.; Fluckiger, B.; Rossi, M. J. The Rate of Water Vapor Evaporation from Ice Substrates in the Presence of HCl and HBr: Implications for the Lifetime of Atmospheric Ice Particles. *Atmos. Chem. Phys.* **2003**, *3*, 1131–1145.
- (36) Delval, C.; Rossi, M. J. Influence of Monolayer Amounts of HNO<sub>3</sub> on the Evaporation Rate of H<sub>2</sub>O over Ice in the Range 179 to 208 K: A Quartz Crystal Microbalance Study. *J. Phys. Chem. A* **2005**, *109*, 7151–7165.
- (37) Pratte, P.; van den Bergh, H.; Rossi, M. J. The Kinetics of H<sub>2</sub>O Vapor Condensation and Evaporation on Different Types of Ice in the Range 130–210 K. *J. Phys. Chem. A* **2006**, *110*, 3042–3058.
- (38) Isono, K.; Iwai, K. Growth Mode of Ice Crystals in Air at Low Pressure. *Nature* **1969**, *223*, 1149.
- (39) Choullarton, T. W.; Latham, J. Measurements of the Deposition Coefficient for Ice, and Its Application to Cirrus Seeding. *Q. J. R. Meteorol. Soc.* **1977**, *103*, 307–318.
- (40) Skrotzki, J.; Connolly, P.; Schnaiter, M.; Saathoff, H.; Möhler, O.; Wagner, R.; Niemand, M.; Ebert, V.; Leisner, T. The Accommodation Coefficient of Water Molecules on Ice–Cirrus Cloud Studies at the AIDA Simulation Chamber. *Atmos. Chem. Phys.* **2013**, *13*, 4451–4466.
- (41) Neshyba, S.; Adams, J.; Reed, K.; Rowe, P. M.; Gladich, I. A Quasi-Liquid Mediated Continuum Model of Faceted Ice Dynamics. *J. Geophys. Res.* **2016**, *121*, 14,035–14,055.
- (42) Mohandesi, A.; Kusalik, P. G. Probing Ice Growth from Vapor Phase: A Molecular Dynamics Simulation Approach. *J. Cryst. Growth* **2018**, *483*, 156–163.
- (43) Llombart, P.; Bergua, R. M.; Noya, E. G.; MacDowell, L. G. Structure and Water Attachment Rates of Ice in the Atmosphere: Role of Nitrogen. *Phys. Chem. Chem. Phys.* **2019**, *21*, 19594–19611.
- (44) Abraham, M. J.; Murtola, T.; Schulz, R.; Páll, S.; Smith, J. C.; Hess, B.; Lindahl, E. GROMACS: High Performance Molecular Simulations through Multi-Level Parallelism from Laptops to Supercomputers. *SoftwareX* **2015**, *1–2*, 19–25.
- (45) Abascal, J.; Sanz, E.; García Fernández, R.; Vega, C. A Potential Model for the Study of Ices and Amorphous Water: TIP4P/Ice. *J. Chem. Phys.* **2005**, *122*, No. 234511.
- (46) Parrinello, M.; Rahman, A. Polymorphic Transitions in Single Crystals: A New Molecular Dynamics Method. *J. Appl. Phys.* **1981**, *52*, 7182–7190.
- (47) Bussi, G.; Donadio, D.; Parrinello, M. Canonical Sampling through Velocity Rescaling. *J. Chem. Phys.* **2007**, *126*, No. 014101.
- (48) Frenkel, D.; Smit, B. *Understanding Molecular Simulation: From Algorithms to Applications*; Elsevier, 2001.
- (49) Humphrey, W.; Dalke, A.; Schulten, K. VMD: Visual Molecular Dynamics. *J. Mol. Graphics* **1996**, *14*, 33–38.
- (50) Willard, A. P.; Chandler, D. Instantaneous Liquid Interfaces. *J. Phys. Chem. B* **2010**, *114*, 1954–1958.
- (51) Errington, J. R.; Debenedetti, P. G. Relationship between Structural Order and the Anomalies of Liquid Water. *Nature* **2001**, *409*, 318.
- (52) Gladich, I.; Pfalzgraff, W.; Maršálek, O.; Jungwirth, P.; Roeselová, M.; Neshyba, S. Arrhenius Analysis of Anisotropic Surface Self-Diffusion on the Prismatic Facet of Ice. *Phys. Chem. Chem. Phys.* **2011**, *13*, 19960–19969.
- (53) Xu, Y.; Petrik, N. G.; Smith, R. S.; Kay, B. D.; Kimmel, G. A. Growth Rate of Crystalline Ice and the Diffusivity of Supercooled Water from 126 to 262 K. *Proc. Natl. Acad. Sci. U.S.A.* **2016**, *113*, 14921–14925.
- (54) Wikfeldt, K. T.; Huang, C.; Nilsson, A.; Pettersson, L. G. M. Enhanced Small-Angle Scattering Connected to the Widom Line in Simulations of Supercooled Water. *J. Chem. Phys.* **2011**, *134*, No. 214506.
- (55) Korolev, A.; McFarquhar, G.; Field, P. R.; Franklin, C.; Lawson, P.; Wang, Z.; Williams, E.; Abel, S. J.; Axisa, D.; Borrmann, S.; Crosier, J.; Fugal, J.; Krämer, M.; Lohmann, U.; Schlenzcek, O.; Schnaiter, M.; Wendisch, M. Mixed-Phase Clouds: Progress and Challenges. *Meteorol. Monogr.* **2017**, *58*, 5.1–5.50.
- (56) Matsuo, S.; Kuniyoshi, H.; Miyake, Y. Vapor Pressure of Ice Containing D<sub>2</sub>O. *Science* **1964**, *145*, 1454–1455.
- (57) Schlesinger, D.; Sellberg, J. A.; Nilsson, A.; Pettersson, L. G. Evaporative Cooling of Microscopic Water Droplets in Vacuo: Molecular Dynamics Simulations and Kinetic Gas Theory. *J. Chem. Phys.* **2016**, *144*, No. 124502.